24th COBEM - 2017

24th ABCM International Congress of Mechanical Engineering
December 3-8, 2017, Curitiba, PR, Brazil

COBEM-2017-1527
COMPARISON BETWEEN PENNES AND DUAL PHASE LAG MODELS FOR THE BIOHEAT TRANSFER AROUND A HEALTHY AND A TUMOROUS THYROID

Tiago Pereira da Costa Bittencourt
Bernard Lamien
Federal University of Rio de Janeiro, PEM/COPPE, Rio de Janeiro, Brazil
tiagopcb@poli.ufrj.br, lamienbernard@hotmail.com

Leonardo Antonio Bermeo Varón
University of Santiago de Cali, School of engineering, bioengineering, Cali, Colombia
lebermeo@gmail.com

Helcio Rangel Barreto Orlande
Federal University of Rio de Janeiro, PEM/COPPE, Rio de Janeiro, Brazil
hrborlande@gmail.com

Abstract. *This work aims to compare two bioheat transfer models – Pennes and Dual Phase Lag (DPL) models – in the computational analysis of the temperature distribution around the thyroid region. This work focuses on the detection of thyroid tumors using measurements of the superficial temperature at the cervical region. Comsol Multiphysics software was used as the simulation platform. Two geometries were utilized in the simulations – normal and deformed ones. The simulated experiment consisted of the application of a thermal stimulation (cooling) on the skin surface of the cervical region, followed by natural heating of the region at room temperature. The conclusions were that Pennes and Dual Phase Lag models describe similarly the temperature distribution in the region analysed. Finally, the results obtained in this work did not reveal any thermal pattern at the skin surface to which could be related the presence of the simulated thyroid tumors.*

Keywords: *Pennes, Dual Phase Lag, bioheat transfer, thyroid, tumor.*

1. INTRODUCTION

Over the last few decades, cancer has become a critical global issue. It is estimated that cancer incidence will increase over the years, majorly in developing countries (Stewart and Wild 2014). For this reason, it is crucial that existing diagnostic and treatment methods are improved and new ones are discovered through innovation and research.

The use of thermal energy on certain therapeutic treatments has been taking place since many years ago (R. W. Y. Habash et al. 2006). However, researches in this field only advanced from the 70's, in laboratories with emphasis in biology and radiation (Diederich 2005). Despite the promising future, technical limitations and issues in reaching proper treatments to kill cells by heating, decreased interest of further research in this field (Dewhirst et al. 2005). This was only regained recently due to the current technological revolution, which has permitted the utilization of nanoparticles (Cheng and Herman 2014; Pirtini Çetingül and Herman 2011; Varon, Orlande, and Eliçabe 2015). Thermal analysis can be conducted for two purposes: treatment (thermal therapy) and diagnostic (thermography).

Hyperthermia – a type of thermal therapy – is the temperature increasing of a specific part of or the whole body above normal for a defined period and for therapeutic purposes. Generally, the temperature range is between 40°C and 45°C (Riadh W Y Habash et al. 2006). This can be undertaken alone or along with other types of cancer treatments. New researches have been undertaken in order to create nanoparticles with appropriate thermal and optical properties capable of concentrating themselves around a tumor and raising its temperature faster than the temperature increase in the healthy tissues nearby, which avoids damage during the treatment (El-Sayed, Huang, and El-Sayed 2005; O'Neal et al. 2004).

Bezerra et al. (2013) defines thermography in medicine as "a simple method which quantifies the body surface temperature by measuring infrared radiation emitted by the human skin." This is done using images captured by thermal cameras. The results might be useful to diagnose anomalies in living beings. (Bezerra et al. 2013; Pirtini Çetingül and

Herman 2011). This is an interesting technique because it is noninvasive, fast, cheap and simple (Bezerra et al. 2013).

The growing interest of the scientific community for this method is due to the modernization of the thermal cameras and the recent revolution in computing and image processing. (Pirtini Çetingül and Herman 2011). Thermography has been utilized already in diagnosis (di Carlo 1995; Cristofolini et al. 1976; Hartmann, Kunze, and Friedel 1981; Santa Cruz et al. 2009). As this is a promising procedure focused on superficial thermal analysis, the use of thermography to diagnose a tumor inside the thyroid can be studied, because the thyroid is located near the skin surface.

According to "Estimativa/2016 - incidência de câncer no Brasil" (2015), thyroid cancer has the higher survival rate. Its diagnosis, although has been constantly improved, is still done by biopsy – an invasive and uncomfortable process, which can take up to one week to generate a result (da Conceição, Lamien, and Orlande 2014; Pirtini Çetingül and Herman 2011). Thus, it is important to research fast and noninvasive techniques for tumor diagnosis. Regarding the cervical region, some dysfunctions such as hyperthyroidism induce a high local temperature variation of the skin over the neck. Therefore, a tumor – when located near the surface – might have the same characteristics and have potential to be diagnosed by thermal analysis (Jin et al. 2014).

Some positive results for other types of cancer have been obtained already (Pirtini Çetingül and Herman 2011). They show promising results of using infrared images to diagnose melanoma. It was concluded that there was a temperature difference between the healthy and tumorous tissues. Jin et al. (2014) developed a tridimensional model based on MRI images related to the pathophysiology of the thyroid. They tried to demonstrate precisely how the thyroid and skin temperatures are affected by blood vessels, breath and thermal stimulus. They conclude that the use of thermography to monitor functional alterations is possible.

Normally, tumors present different properties from healthy tissues. They present higher metabolic activities and blood perfusion so that tumor temperature is higher than healthy tissues temperature (Song 1984). This happens because the tumor has a chaotic growth, so cells and blood vessels grow uncontrollably (Pirtini Çetingül and Herman 2011). There are two types of thermography: the static and the dynamic methods (Cetingül and Herman 2010). In the static IR imaging, the images are collected when the analyzed region is at the steady state. In the dynamic IR imaging, the images are obtained after the application of a stimulus (heating or cooling) in the region of interest in order to induce and/or enhance thermal contrasts (Pirtini Çetingül and Herman 2011). The static method is not the best option for this study, because it requires a long period until the body reaches the steady sate. Besides, depending on the location and size of the tumor, the thermal contrast between both tissues are generally smaller in the steady state rather than in the transient regime (Cheng and Herman 2014). Thus, it is more interesting to do the IR imaging with the application of thermal stimulus, as it gives more contrast (Pirtini Çetingül and Herman 2011; Santa Cruz et al. 2009). Santa Cruz et al. (2009) attribute the first application of IR imaging with thermal stimulus aiming thermal contrast to an Italian group (di Carlo 1995).

Bioheat transfer is a complex phenomenon due to the strong influence of the blood circulation and the heat generated by metabolism. These influences have been studied for more than a century (Lakhssassi, Kengne, and Semmaoui 2010). The first model to take into account the metabolism, blood flow, conduction and external sources of heat was proposed by Pennes in 1948 (Pennes 1948). Pennes lumped the cooling effects of blood flow in the perfusion term (Pennes 1948). Effects of blood perfusion are proportional to the temperature difference between arterial blood and the tissue. Even though Pennes model is widely utilized, it presents some limitations. Xuan and Roetzel (1997), (1998) modified the Pennes model with the theory of porous media. Some limitations of the Pennes model have to do with the assumptions presented in the bioheat equation. Pennes model is derived from Fourier's law (Eq. (1)).

$$\mathbf{q} = -k\nabla T \tag{1}$$

Fourier's law assumes that the heat propagation speed in the tissue is infinite (Ordóñez-Miranda and Alvarado-Gil 2010; Poor, Moosavi, and Moradi 2014). Fourier's law is known to fail in some cases, including processes with fast transients, small spatial scales or at extremely low temperatures (Ordóñez-Miranda and Alvarado-Gil 2010; Poor, Moosavi, and Moradi 2014). Blood and tissues are not in thermal equilibrium. Thus, blood exchanges heat with the tissue, generating a delay between the temperature gradient and the heat flux. Some models derived from Pennes equation are proposed to overcome these issues such as the Dual Phase Lag model (DPL) and the model of the thermal wave.

The model of the thermal wave was developed, independently, by Cattaneo (1958) and Vernotte (1958). In this model, the Fourier law was modified in order to take into account the finite speed of heat propagation, resulting in a hyperbolic heat conduction equation with a wave behavior. Although Cattaneo-Vernotte's model eliminates the infinite speed issue, it does not eliminate the existence of an instantaneous response between the temperature gradient and the energy transport. Besides, it assumes that the temperature gradient is always the cause and heat transfer the effect (Majchrzak 2010; Tzou 2014). In order to overcome these last problems, Tzou proposed the Dual Phase Lag (DPL) model (Tzou 2014; Tzou 1989). The bioheat transfer model that results from the DPL constitutive equation is given by (Majchrzak 2010; Majchrzak and Turchan 2015; Tzou 2014; Tzou 1989):

$$c(x,y,z)\left[\frac{\partial T(x,y,z,t)}{\partial t}+\frac{\tau_q\partial^2 T(x,y,z,t)}{\partial t^2}\right]=\nabla.\left[k(x,y,z)\nabla T(x,y,z,t)\right]+\frac{k(x,y,z)\tau_t\partial\nabla^2 T(x,y,z,t)}{\partial t}+$$
$$+\rho_b c_b\omega_b(x,y,z)\left[T_b-T(x,y,z,t)\right]+Q_m(x,y,z,t)+\frac{\tau_q\partial\left\{\rho_b c_b\omega_b(x,y,z)\left[T_b-T(x,y,z,t)\right]+Q_m(x,y,z,t)\right\}}{\partial t} \quad (2)$$

where ρ, c and k represent the specific mass, the specific heat and the thermal conductivity of the tissue, respectively; the subscript "b" is used for the blood properties. ω_b is the blood perfusion coefficient and Q_m is the generated heat from the metabolic activity. T_b represents the temperature of arterial blood and T represents the temperature of the tissue in a determined point and time. τ_q is the relaxation time and τ_t is thermalization time, which can be interpreted as the time that it takes to generate a temperature gradient after the beginning of the heat conduction (Xu, Seffen, and Lu 2008). Thus, the determination of cause and effect depends on the magnitudes of relaxation and thermalization times.

When $\tau_q < \tau_t$, heat flux induces the temperature gradient and when the opposite happens, the temperature gradient generates a heat flux through the material (Ordóñez-Miranda and Alvarado-Gil 2010). This work aims to compare the Pennes and Dual Phase Lag models for bioheat transfer in a computational analysis of the temperature distribution around the thyroid region with and without a tumor, as presented next.

2. PHYSICAL MODEL AND MATHEMATICAL FORMULATION

For the physical problem of interest in this work, a thermal perturbation is applied over the cervical region, which is maintained at a low temperature during a cooling period. The comparison of the two models is then performed during the reheating period, when the skin exchanges heat with the surrounding environment by natural convection and linearized radiation at room temperature. Therefore, the analysis was executed in three different periods: steady state before cooling, cooling and reheating. The duration of the cooling period was of 30 seconds, when the skin was kept at constant temperature of 0°C. The duration of the reheating period was taken as 300 seconds.

The geometry of the cervical region of interest was created in SolidWorks (Fig. 1 and Fig. 2). It consists of a simplified model of a section of the human neck. In the geometry with the healthy thyroid, the glandule is placed over the trachea, which serves as part of the internal boundary surface. Muscle is assumed as the tissue directly over the thyroid, which is covered by layers of fat and skin, respectively. In the other geometry examined in this work, the thyroid is distorted by the presence of a tumor, which is considered as an ellipsoid as illustrated by Fig. 1 (da Conceição 2014). The carotid arteries and the jugular veins are not considered in the analysis.

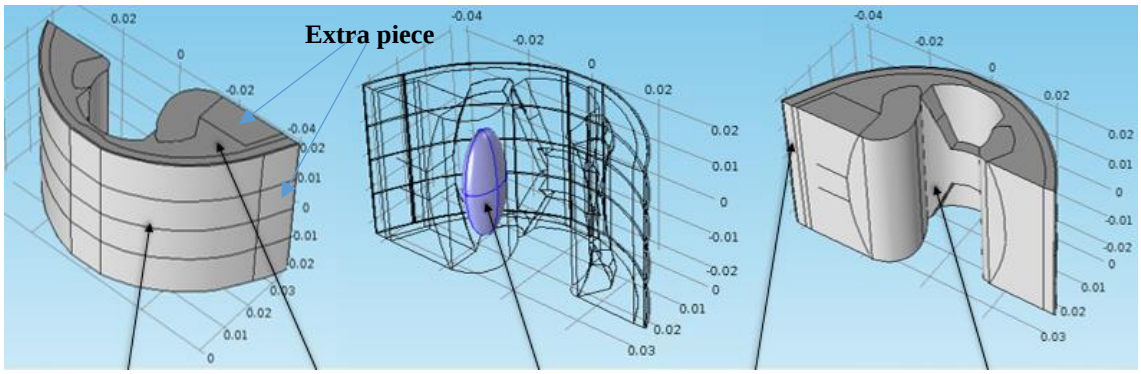

Figure 1. Deformed geometry with distorted thyroid and a tumor.

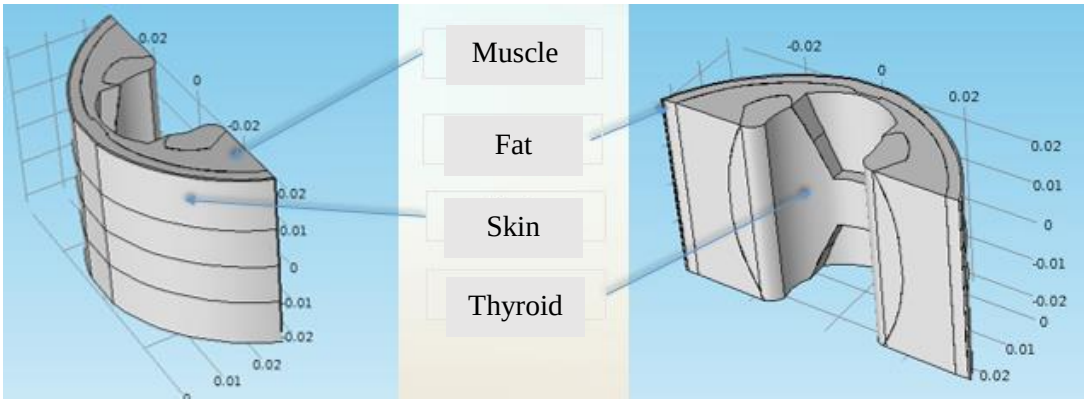

Figure 2. Normal geometry with healthy thyroid modelled in SolidWorks.

As described before, the numerical simulations involved three periods – steady state before cooling, cooling and reheating. In the first period, natural convection and linearized radiation was assumed as the boundary condition of the skin surface (Γ_2). The remaining surfaces (Γ_1) were assumed insulated. In the second period (cooling), constant temperature was chosen as the boundary condition of the skin surface (Γ_2). The remaining surfaces (Γ_1) were assumed insulated. In the third period, the assumptions regarding boundary conditions were the same of the first period. The surfaces Γ_1 and Γ_2, together with the arches utilized for obtaining the results are shown in Fig. 3.

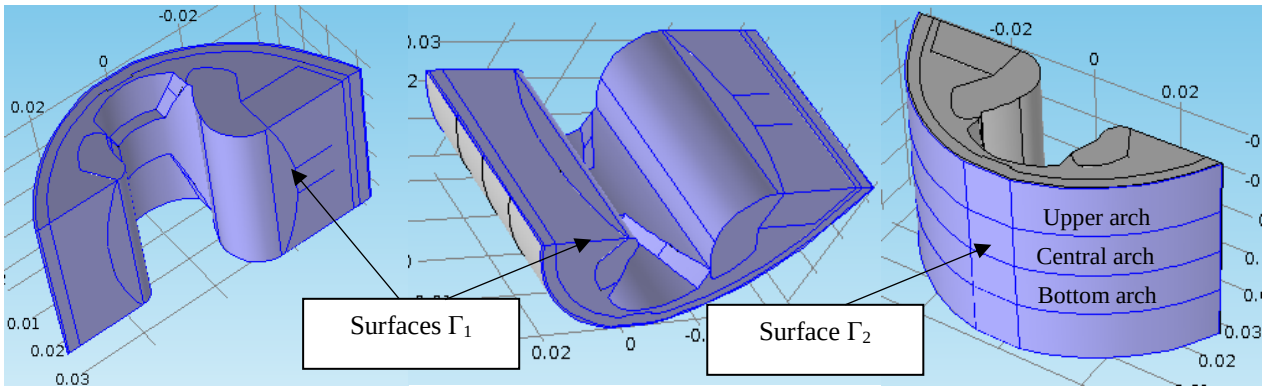

Figure 3. Surfaces Γ_1 and Γ_2 labelled and highlighted in blue. Arches used in the simulations labelled. The surfaces and arches are the same, independently of the geometry utilized.

2.1. PENNES MODEL

For the steady state before the cooling period, the mathematical formulation for the problem is given by:

$$0 = \nabla.\left[k(x,y,z)\nabla T(x,y,z)\right] + \rho_b c_b \omega_b(x,y,z)\left[T_b - T(x,y,z)\right] + Q_m(x,y,z) \tag{3}$$

$$x,y,z \in \Gamma_1 : -\mathbf{n}\cdot k(x,y,z)\nabla T(x,y,z) = 0 \tag{4}$$

$$x,y,z \in \Gamma_2 : -\mathbf{n}\cdot k(x,y,z)\nabla T(x,y,z) = h(T_{ext} - T(x,y,z)) \tag{5}$$

For the cooling period:

$$\rho(x,y,z)c(x,y,z)\frac{\partial T(x,y,z,t)}{\partial t} = \nabla\cdot\left[k(x,y,z)\nabla T(x,y,z,t)\right] + \rho_b c_b \omega_b(x,y,z)\left[T_b - T(x,y,z,t)\right] + Q_m(x,y,z,t) \tag{6}$$

$$x,y,z \in \Gamma_1 : -\mathbf{n}\cdot k(x,y,z)\nabla T(x,y,z,t) = 0 \tag{7}$$

$$x,y,z \in \Gamma_2 : T(x,y,z,t) = 273.15\ \text{K},\ 0 \le t \le 30\ \text{s} \tag{8}$$

Initial Condition: Temperature distribution obtained from the previous period.

For the reheating period:

$$\rho(x,y,z)c(x,y,z)\frac{\partial T(x,y,z,t)}{\partial t} = \nabla\cdot\left[k(x,y,z)\nabla T(x,y,z,t)\right] + \rho_b c_b \omega_b(x,y,z)\left[T_b - T(x,y,z,t)\right] + Q_m(x,y,z,t) \tag{9}$$

$$x,y,z \in \Gamma_1 : -\mathbf{n}\cdot k(x,y,z)\nabla T(x,y,z,t) = 0 \tag{10}$$

$$x,y,z \in \Gamma_2 : -\mathbf{n}\cdot k(x,y,z)\nabla T(x,y,z,t) = h(T_{ext} - T(x,y,z,t)) \tag{11}$$

Initial condition: temperature distribution obtained at the end of the previous period.

where (Majchrzak and Turchan 2015):

$$Q_m = Q_{met} 3^{\frac{T(x,y,z,t)-T_b}{10}} \tag{12}$$

2.2. DPL MODEL

For the steady state before the cooling period, the mathematical formulation with the DPL model is identical to that with Pennes' model, since the DPL constitutive equation is identical to Fourier´s law at steady state. Therefore, Eq. (3) to Eq. (5) are used for the steady state problem for the DPL model.

For the cooling period:

$$c(x,y,z)\left[\frac{\partial T(x,y,z,t)}{\partial t} + \frac{\tau_q \partial^2 T(x,y,z,t)}{\partial T^2}\right] = \nabla\cdot\left[k(x,y,z)\nabla T(x,y,z,t)\right] + \frac{k(x,y,z)\tau_t \partial \nabla^2 T(x,y,z,t)}{\partial t} + \\ + \rho_b c_b \omega_b(x,y,z)\left[T_b - T(x,y,z,t)\right] + Q_m(x,y,z,t) + \frac{\tau_q \partial\left\{\rho_b c_b \omega_b(x,y,z)\left[T_b - T(x,y,z,t)\right] + Q_m(x,y,z,t)\right\}}{\partial t} \tag{13}$$

$$x,y,z \in \Gamma_1 : -\mathbf{n}\cdot k(x,y,z)\nabla T(x,y,z,t) - \frac{k(x,y,z)\tau_t \partial n \nabla T(x,y,z,t)}{\partial t} = 0 \tag{14}$$

$$x,y,z \in \Gamma_2 : T(x,y,z,t) = 273.15\ \text{K},\ 0 \le t \le 30\ \text{s} \tag{15}$$

For the reheating period:

$$c(x,y,z)\left[\frac{\partial T(x,y,z,t)}{\partial t} + \frac{\tau_q \partial^2 T(x,y,z,t)}{\partial T^2}\right] = \nabla\cdot\left[k(x,y,z)\nabla T(x,y,z,t)\right] + \frac{k(x,y,z)\tau_t \partial \nabla^2 T(x,y,z,t)}{\partial t} + \\ + \rho_b c_b \omega_b(x,y,z)\left[T_b - T(x,y,z,t)\right] + Q_m(x,y,z,t) + \frac{\tau_q \partial\left\{\rho_b c_b \omega_b(x,y,z)\left[T_b - T(x,y,z,t)\right] + Q_m(x,y,z,t)\right\}}{\partial t} \tag{16}$$

$$x,y,z \in \Gamma_1 : -\mathbf{n}\cdot k(x,y,z)\nabla T(x,y,z) - \frac{k(x,y,z)\tau_t \partial n \nabla T(x,y,z,t)}{\partial t} = 0 \tag{17}$$

$$x,y,z \in \Gamma_2 : -\mathbf{n}\cdot k(x,y,z)\nabla T(x,y,z,t) - \frac{k(x,y,z)\tau_t \partial n \nabla T(x,y,z,t)}{\partial t} = h(T_{ext} - T(x,y,z,t)) + \\ + \frac{\tau_q \partial(h(T_{ext} - T(x,y,z,t)))}{\partial t} \tag{18}$$

Initial condition: temperature distribution obtained at the end of the previous period.

3. RESULTS AND DISCUSSIONS

The thermophysical properties were mainly obtained from (Ghanbari and Hajj 2013; Hasgall et al. 2013; Lamien 2015). Based on literature data and other types of tumor, the metabolic heat source of the thyroid was set to 10 times the metabolic heat source of a healthy thyroid (Bittencourt 2017). It is very difficult to obtain values for the thermalization and relaxation times. The calculation of these terms are also beyond the scope of this work.

One alternative found was to select three values (0.5, 1 and 5 s) among a range of typical values for these two terms for general living tissues (Bittencourt 2017; Zhang 2009; Zhou, Zhang, and Chen 2009). Therefore, a parametric analysis was undertaken in this work in order to understand how relaxation and thermalization times affect the bioheat transfer. In this study, it was considered T_{ext} = 25°C and h = 10 W/(m^2.K) (Cheng and Herman 2014). The software Comsol Multiphysics 5.0 was utilized to solve the equations presented before (Eq. (3) to Eq. (18)). Results are presented for three distinct arches pictured in Fig. 3.

As Comsol does not have the DPL model in its library, Eq. (13) to Eq. (18) had to be inserted manually in the software. Thus, it was required to verify these equations. The results from Majchrzak and Turchan (2015) were used for verification purposes (Bittencourt 2017). A mesh convergence analysis was performed, indicating that the so-called "normal mesh" (generated automatically on Comsol). The computational time for 30 seconds of simulation utilizing the Pennes model in the reheating period was 2 minutes and 10 seconds with the "normal mesh" (66,243 elements); 16 minutes and 36 seconds with the "finer mesh" (309,602 elements) and 39 minutes and 16 seconds with the "extra fine mesh" (558913 elements). For the interpretation of the different results presented below, we summarized in Table 1 the meaning of the acronyms appearing in the legends used in the figures.

Table 1. Table containing the acronyms utilized in the graphs' legends with their respective meanings.

Acronyms	**Meaning**
PST	Pennes' model without tumor
DST 0.5	DPL model without tumor with $\tau_q = \tau_t = 0.5$
DST 1	DPL model without tumor with $\tau_q = \tau_t = 1$
DST 5	DPL model without tumor with $\tau_q = \tau_t = 5$
PCT	Pennes' model with tumor
DCT 0.5	DPL model with tumor with $\tau_q = \tau_t = 0.5$
DCT 1	DPL model with tumor with $\tau_q = \tau_t = 1$
DCT 5	DPL model with tumor with $\tau_q = \tau_t = 5$
PST e	Pennes' model for the deformed geometry without tumor

In order to investigate how the geometry affects the results, firstly, a simulation was undertaken utilizing both models and both geometries – normal (Fig. 1) and deformed (Fig. 2) – in all the three periods. The results for the steady state are presented in Fig. 4 and for the reheating period in Fig. 5 to Fig. 8. Figure 4 contains the curves of temperature distribution along the central arch for both geometries at the steady state.

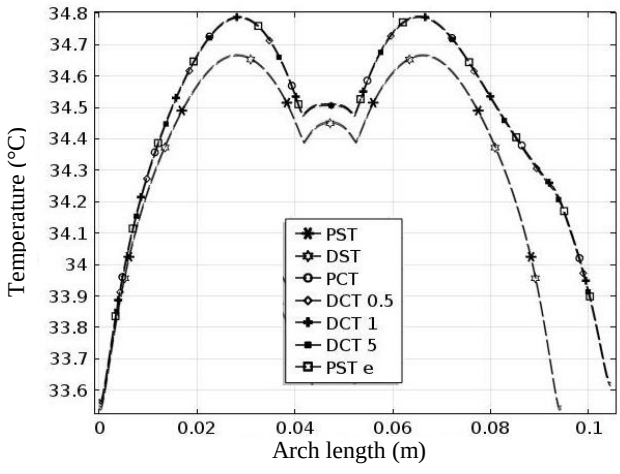

Figure 4. Temperature distribution along the central arch for the normal geometry (without tumor) and the deformed geometry (with and without tumor) in the steady state.

The curves presented in Fig. 4 for the same geometry that were generated by different models are superimposed. In addition, the temperature distribution along the central arches for different geometries are distinct from each other. The temperature distribution for the deformed geometry reach higher temperature values. One simulation was performed utilizing the deformed geometry without tumor and was included in Fig. 4. The curve of this simulation superimpose with its corresponding curves (belonging to the deformed geometry). Therefore, it can be preliminarily concluded that a distortion in the geometry affects the temperature distribution along the skin surface. In addition, at the steady state, the results are the same no matter what model is being used.

In the reheating period, the results for the normal geometry were first analyzed as presented in Fig. 5. Figure 5 shows that as τ_q and τ_t increase, the difference between the two modes decrease as the simulation progress in time, because the transient effects die out. It is interesting to note that the shapes of the curves obtained with DPL and Pennes' models are the same, although the temperature increases are not the same.

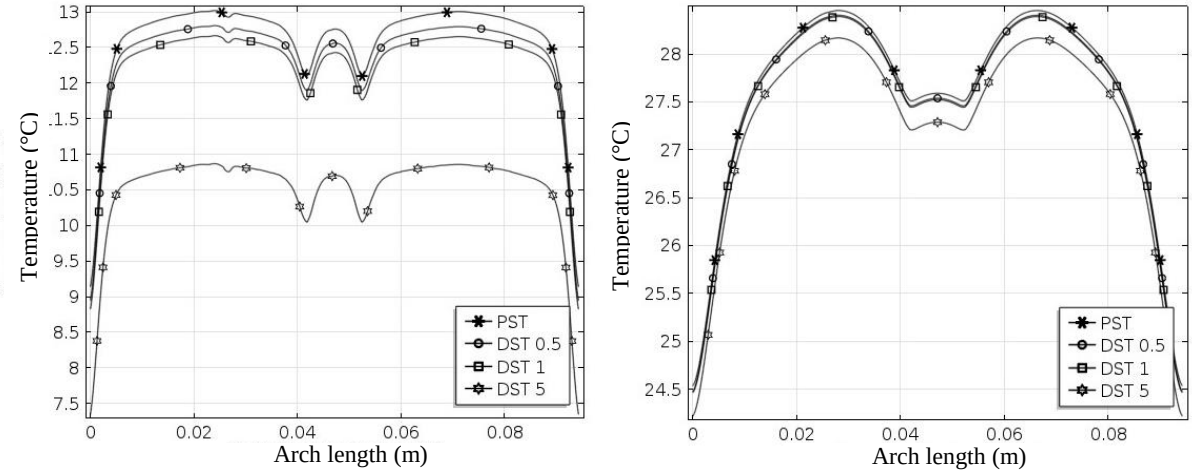

Figure 5. Temperature distribution along the central arch of the normal geometry without a tumor at the reheating period, at 20 and 150 seconds of simulation.

Other simulations were then performed using only the deformed geometry with and without a tumor. The aim was to examine if it is possible to detect a tumor by temperature measurements of the skin surface. Figure 6 shows the temperature distribution at the reheating period along the central arch for the deformed geometry, with and without a tumor. The temperature distribution of the deformed geometry (without tumor) skin surface has a similar behaviour of the temperature distribution containing a tumor.

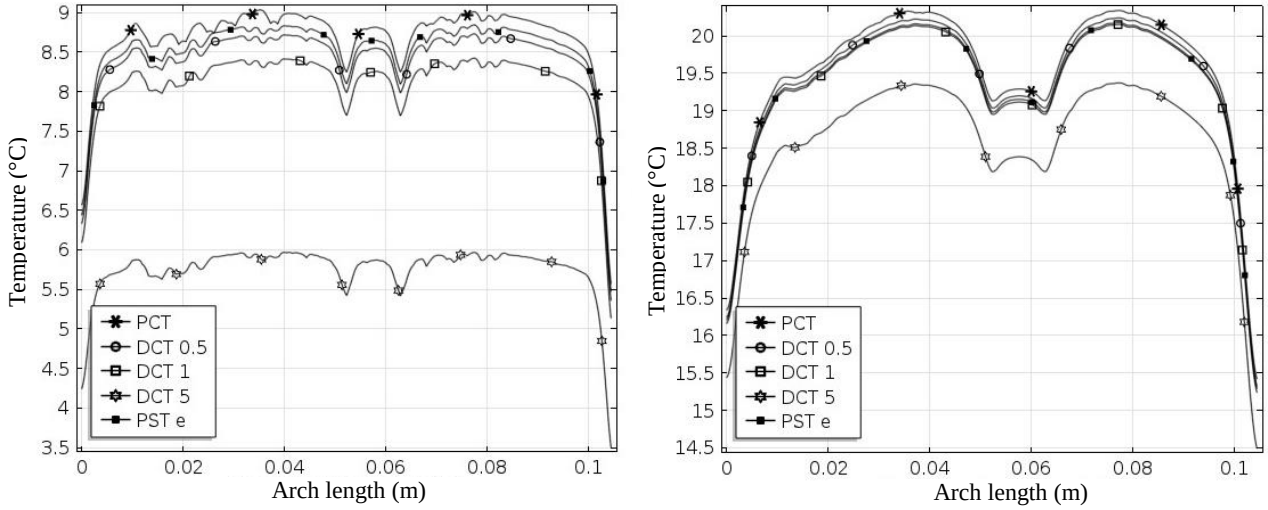

Figure 6. Temperature distribution along the central arch of the deformed geometry at the reheating period, at 10 and 50 seconds of simulation.

Figure 7 presents the temperature distribution of the central arch for the deformed geometry (with and without tumor) and the normal geometry (without tumor), during the reheating period at times 10 and 20 seconds. The temperature differences between the cases with and without a tumor are quite small. Therefore, measurement techniques with quite

small uncertainties would be required to detect the tumor from the surface temperature. Infrared thermography with nowadays cameras can provide measurements with quite small uncertainties, when the surface emissivity is accurately known. On the other hand, the emissivity of the skin can change from individual to individual and even for the same individual under different physiological and skin conditions, which might result in difficulties for the tumor detection by thermography measurements.

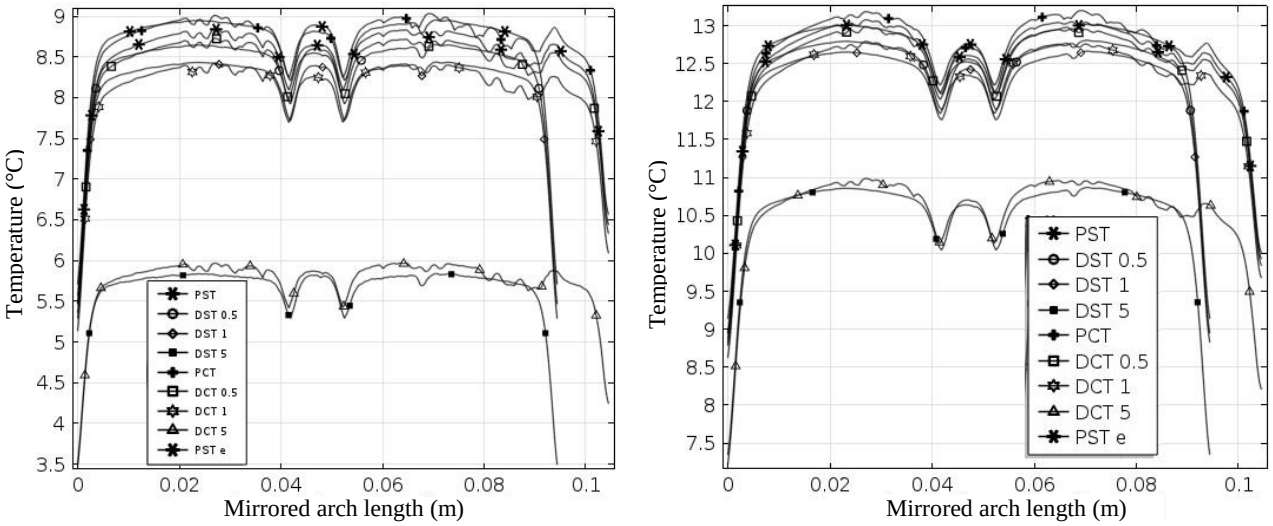

Figure 7. Temperature distribution of the central arch of the deformed geometry (with and without tumor) and the normal geometry (without tumor) at the reheating period, at 10 and 20 seconds of simulation.

Figure 8 shows curves of temperature distribution along the central arch of the deformed geometry in the reheating period at 10 and 30 seconds. It can be observed in Fig. 8 that the temperature profiles of the cases with and without tumors are superimposed. This means that the tumor does not affect the temperature distribution over the skin, regardless of the heat conduction problem used in the analysis. One possible reason for the lack of influence of the tumor on the temperature distribution of the skin surface is the fat layer. Due to its low thermal conductivity, fat works like a thermal insulator.

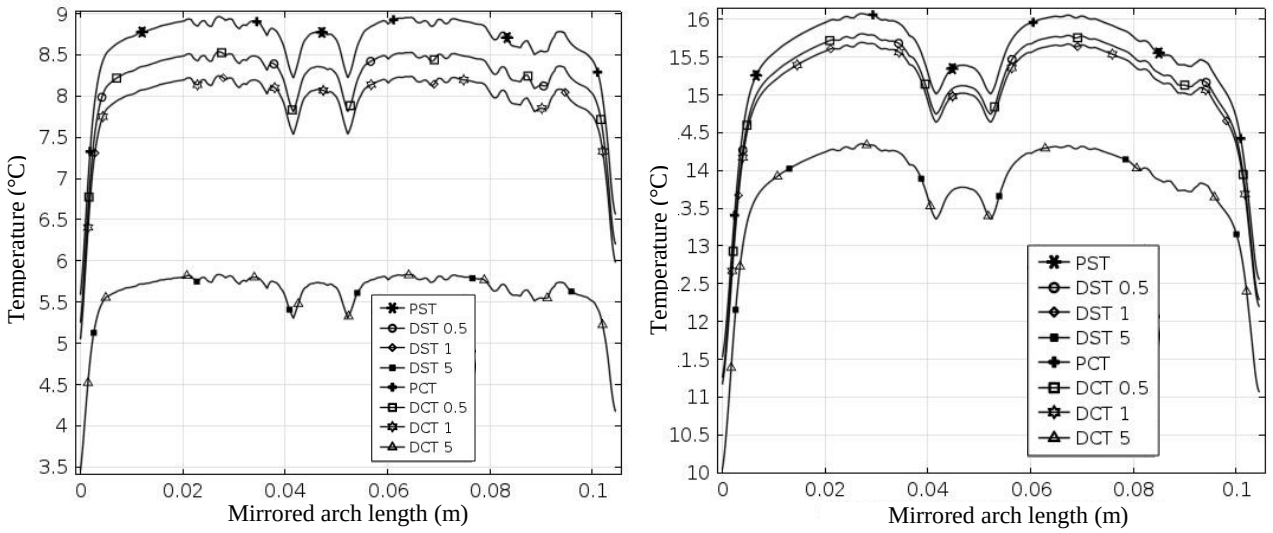

Figure 8. Temperature distribution along the central arch of the deformed geometry (with and without tumor) at the reheating period, at 10 and 30 seconds of simulation.

4. CONCLUSIONS

A numerical analysis of bioheat transfer models was performed in this work, with focus on the analysis of the surface temperature of the cervical region around the thyroid. Both Pennes‘ model and the Dual Phase Lag model were implemented and compared for cases involving thyroids with and without a tumor. As the relaxation times in the dual phase lag model increase the observed temperature increase during reheating is smaller. On the other hand, the difference between the two models decrease as the simulation progresses in time, because the transient effects die out, and the effects of the relaxation times become smaller. Hence, the effects of the relaxation times are to lag the temperature response during the reheating period. For the several analyzed cases, no significant temperature difference was observed when the thyroid included a tumor or not. Therefore, measurement techniques with quite small uncertainties would be required to detect the tumor from the surface temperature. Infrared thermography with nowadays cameras can provide measurements with quite small uncertainties, when the surface emissivity is accurately known. On the other hand, the emissivity of the skin can change from individual to individual and even for the same individual under different physiological and skin conditions, which might result in difficulties for the tumor detection by thermography measurements.

5. ACKNOWLEDGMENTS

CNPq, CAPES and FAPERJ supported this work.

6. REFERENCES

Bezerra, L. A., Oliveira, M. M., Rolim, T. L., Conci, A., Santos, F. G. S., Lyra, P. R. M., and Lima, R. C. F. 2013. “Estimation of Breast Tumor Thermal Properties Using Infrared Images”. *Signal Processing* 93(10): 2851–63. http://dx.doi.org/10.1016/j.sigpro.2012.06.002.

Bittencourt, T. P. da C. 2017. *Comparação Entre O Modelo de Pennes e de Duplo Retardo Para a Biotransferência de Calor Na Região Ao Redor Da Tireoide*. BEng thesis, Federal University of Rio de Janeiro, Brazil.

Cattaneo, C. 1958. “A Form of Heat Conduction Equation Which Eliminates the Paradox of Instantaneous Propagation”. *Comp. Rend.* 247: 431–33.

Cetingül, M. P., and Herman, C. 2010. “A Heat Transfer Model of Skin Tissue for the Detection of Lesions: Sensitivity Analysis”. *Physics in medicine and biology* 55(19): 5933–51.

Cheng, T. Y. and Herman, C. 2014. “Analysis of Skin Cooling for Quantitative Dynamic Infrared Imaging of near-Surface Lesions”. *International Journal of Thermal Sciences* 86: 175–88.

Cristofolini, M., Piscioli, F., Valdagni, C., and Della Selva, A. 1976. “Correlations between Thermography and Morphology of Primary Cutaneous Malignant Melanomas”. *Acta Thermogr* 1(1): 3–11.

da Conceição, D. S. 2014. *Temperatura Na Região Cervical Ao Redor Da Tireóide Com E Sem a Presença de Um Tumor*. BEng. thesis, Federal University of Rio de Janeiro, Brazil.

da Conceição, D. S., Lamien, B. and Orlande, H. R. B. 2014. “Computational Analysis of the Temperature Distribution in the Cervical Region Around a Normal or a Tumorous Thyroid”. In *Proceedings of 15th Brazilian Congress of Thermal Sciences and Engineering*: 13–16. Belém, Brazil.

Dewhirst, M. W., Vujaskovic, Z., Jones, E., and Thrall, D. 2005. “Re-Setting the Biologic Rationale for Thermal Therapy”. *International Journal of Hyperthermia* 21(12): 779–90.

di Carlo, A. 1995. “Thermography and the Possibilities for Its Applications in Clinical and Experimental Dermatology”. *Clinics in Dermatology* 13(4): 329–36.

Diederich, C. J. 2005. “Thermal Ablation and High-Temperature Thermal Therapy: Overview of Technology and Clinical Implementation”. *International Journal of Hyperthermia* 21(8): 745–53.

El-Sayed, I. H., Huang, X. and El-Sayed, M. A.. 2005. “Surface Plasmon Resonance Scattering and Absorption of Anti-EGFR Antibody Conjugated Gold Nanoparticles in Cancer Diagnostics: Applications in Oral Cancer”. *Nano letters* 5(5): 829–34.

Estimativa/2016, 2015. “Incidência de Câncer No Brasil”. Instituto Nacional de Cancer José Alencar Gómez Dasilva, INCA, Rio de Janeiro. <http://www.inca.gov.br/bvscontrolecancer/publicacoes/edicao/Estimativa_2016.pdf>

Ghanbari, P. and M. Hajj. 2013. “Finite Element Analysis of Tissue Electropermeability through the Application of Electric Pulses”. *J Bioengineer & Biomedical Sci* 3(120): 2.

Habash, R. W. Y., Bansal, R., Krewski, D., and Alhafid, H. T. 2006. “Thermal Therapy, Part 1 : An Introduction to Thermal Therapy”. *Critical Reviews in Biomedical Engineering* 34(6): 459–89.

Habash, R. W. Y., Bansal, R., Krewski, D., and Alhafid, H. T. 2006. “Thermal Therapy, Part 2 : Hyperthermia Techniques”. *Critical Reviews in Biomedical Engineering* 34(6): 491–542.

Hartmann, M., Kunze, J., and Friedel, S. 1981. “Telethermography in the Diagnostics and Management of Malignant Melanomas”. *The Journal of dermatologic surgery and oncology* 7(3): 213–18.

Hasgall P.A, Di Gennaro F, Baumgartner C, Neufeld E, Gosselin M.C, Payne D, Klingenböck A, Kuster N, 2015. “IT’IS Database for thermal and electromagnetic parameters of biological tissues,” Version 3.0, <http://www.itis.ethz.ch/>.

Jin, C., He, Z. Z., Yang, Y., and Liu, J. 2014. "MRI-Based Three-Dimensional Thermal Physiological Characterization of Thyroid Gland of Human Body". *Medical Engineering and Physics* 36(1): 16–25.

Lakhssassi, A., Kengne, E. and Semmaoui, H. 2010. "Modifed Pennes' Equation Modelling Bio-Heat Transfer in Living Tissues: Analytical and Numerical Analysis". *Natural Science* 2(12): 1375–85.

Lamien, B. 2015. *Problema de Estimativa de Estado no Tratamento de Câncer por Hipertermia com Aquecimento por Laser Diodo na Faia do Infravermelho*. DSc. thesis, Federal University of Rio de Janeiro, Brazil.

Majchrzak, E. 2010. "Numerical Solution of Dual Phase Lag Model of Bioheat Transfer Using the General Boundary Element Method". *Computer Modeling in Engineering and Sciences* 69(1): 43.

Majchrzak, E. and Turchan, L. 2015. "The General Boundary Element Method for 3D Dual-Phase Lag Model of Bioheat Transfer". *Engineering Analysis With Boundary Elements* 50: 76–82.

O'Neal, D. P., Hirsch, L. R., Halas, N. J., Payne, J. D., and West, J. L. 2004. "Photo-Thermal Tumor Ablation in Mice Using near Infrared-Absorbing Nanoparticles". *Cancer letters* 209(2): 171–76.

Ordóñez-Miranda, J. and Alvarado-Gil, J. J. 2010. "Determination of Time-Delay Parameters in the Dual-Phase Lagging Heat Conduction Model". *Journal of Heat Transfer* 132(6): 61302.

Pennes, H. H. 1948. "Analysis of Tissue and Arterial Blood Temperatures in the Resting Human Forearm". *Journal of Applied Physiology* 1(9): 93–122.

Pirtini Çetingül, M. and Herman, C. 2011. "Quantification of the Thermal Signature of a Melanoma Lesion". *International Journal of Thermal Sciences* 50(4): 421–31.

Poor, H. Z., Moosavi, H. and Moradi, A. 2014. "Investigation on the Dual-Phase Lag Effects in Biological Tissues during Laser Irradiation". *Int. J. Mech. Sust. Eng.* 4(November): 33–46.

Santa Cruz, G. A., Bertotti, J., Marín, J., González, S. J., Gossio, S., Alvarez, D., Roth, B. M. C., Menéndez, P., Pereira, M. D., Albero, M., Cubau, L., Orellano, P., and Liberman, S.J. 2009. "Dynamic Infrared Imaging of Cutaneous Melanoma and Normal Skin in Patients Treated with BNC". *Applied radiation and isotopes : including data, instrumentation and methods for use in agriculture, industry and medicine* 67(7–8 Suppl): S54–58.

Song, C. W. 1984. "Effect of Local Hyperthermia on Blood Flow and Microenvironment: A Review". *Cancer research* 44(10 Supplement): 4721s–4730s.

Stewart, B. and Wild, C. P. 2014. "World Cancer Report 2014". 2014.

Tzou, D. Y. 2014. *Macro-to Microscale Heat Transfer: The Lagging Behavior*. John Wiley & Sons.

Varon, L. A. B., Orlande, H. R. B. and Eliçabe, G. E. 2015. "Estimation of State Variables in the Hyperthermia Therapy of Cancer with Heating Imposed by Radiofrequency Electromagnetic Waves". *International Journal of Thermal Sciences* 98: 228–36.

Vernotte, P. 1958. "Les Paradoxes de La Théorie Continue de Léquation de La Chaleur". *Comptes Rendus Hebdomadaires Des Seances De L Academie Des Sciences* 246(22): 3154–55.

Xu, F., Seffen, K. A. and Lu, T. J. 2008. "Non-Fourier Analysis of Skin Biothermomechanics". *International Journal of Heat and Mass Transfer* 51(9): 2237–59.

Xuan, Y. and Roetzel, W., 1997. "Bioheat Equation of the Human Thermal System". *Chemical engineering & technology* 20(4): 268–76.

Xuan, Y. and Roetzel, W., 1998. "Transient Response of the Human Limb to an External Stimulust". *International Journal of Heat and Mass Transfer* 41(1): 229-39.

Zhang, Y. 2009. "Generalized Dual-Phase Lag Bioheat Equations Based on Nonequilibrium Heat Transfer in Living Biological Tissues". *International Journal of Heat and Mass Transfer* 52(21–22): 4829–34.

Zhou, J., Zhang, Y. and Chen, J. K. 2009. "An Axisymmetric Dual-Phase-Lag Bioheat Model for Laser Heating of Living Tissues". *International Journal of Thermal Sciences* 48(8): 1477–85.

7. RESPONSIBILITY NOTICE

The authors are the only responsible for the printed material included in this paper.